Image and Vision Computing 29 (2011) 631–637

Contents lists available at ScienceDirect

Image and Vision Computing

journal homepage: www.elsevier.com/locate/imavis

Median-based image thresholding ☆

Jing-Hao Xue [a,*], D. Michael Titterington [b]

[a] Department of Statistical Science, University College London, London WC1E 6BT, UK
[b] School of Mathematics and Statistics, University of Glasgow, Glasgow G12 8QQ, UK

ARTICLE INFO

Article history:
Received 11 November 2010
Received in revised form 24 March 2011
Accepted 12 June 2011

Keywords:
Image segmentation
Image thresholding
Laplace distributions
Mean absolute deviation from the median (MAD)
Minimum error thresholding (MET)
Otsu's method

ABSTRACT

In order to select an optimal threshold for image thresholding that is relatively robust to the presence of skew and heavy-tailed class-conditional distributions, we propose two median-based approaches: one is an extension of Otsu's method and the other is an extension of Kittler and Illingworth's minimum error thresholding. We provide theoretical interpretation of the new approaches, based on mixtures of Laplace distributions. The two extensions preserve the methodological simplicity and computational efficiency of their original methods, and in general can achieve more robust performance when the data for either class is skew and heavy-tailed. We also discuss some limitations of the new approaches.

1. Introduction

Image thresholding aims to partition an image into K predetermined, mutually-exclusive classes, C_1, ..., C_K, based on $K-1$ intensity thresholds. Most commonly, $K=2$ and the image is partitioned into the background and the foreground. As an initial procedure for realising image segmentation, thresholding has a long history of investigation, motivated by a broad range of practical applications of image analysis and object recognition. Comprehensive overviews and comparative studies of image thresholding can be found in [15,4,17,16], for example.

Many, and the most-widely used, approaches to image thresholding are based on analysis of the histogram of intensities in an image, searching for an optimal threshold t^* to divide the histogram into two parts, C_1 with intensities lower than t^* and C_2 for the remainder.

Among these approaches, two of the most popular are Otsu's method [12] and Kittler and Illingworth's minimum-error-thresholding (MET) method [8]. Otsu's method is adopted as the method for automatic image thresholding in some free and commercial software, such as GIMP (www.gimp.org) and MATLAB (The MathWorks, Inc.). The MET method is ranked as the best in a comprehensive survey of image thresholding conducted by [16].

In image thresholding, determination of an optimal threshold t^* is often based on the estimation of measures of location and dispersion of intensities in C_1 and C_2. As with many other approaches, both Otsu's method and the MET method use the sample mean and the sample standard deviation to estimate location and dispersion, respectively.

It is well known that, when the distribution for class C_k is skew or heavy-tailed, or when there are outliers in the sample from C_k, the median is a more robust estimator of location than the mean. When the median is chosen for location, the mean absolute deviation from the median (denoted by MAD) is usually chosen as the estimator of dispersion.

Therefore, in order to select a t^* that is more robust to the presence of skew and heavy-tailed distributions for C_k than those selected by Otsu's method and the MET method, we propose in section 2 two median-based approaches to image thresholding. One of them is an extension of Otsu's method and the other is an extension of the MET method; both methods are based on the use of the MAD. Like their original versions, the two new approaches remain methodologically simple and computationally efficient.

The relationship between Otsu's method and the MET method has been investigated by [9,21], among others. [9] shows that both methods can be derived from maximisation of log-likelihoods based on mixtures of Gaussian distributions. In section 3, we present theoretical interpretation of their median-based extensions from the perspective of the maximisation of log-likelihoods for mixtures of Laplace distributions.

Some limitations of the median-based approaches are discussed in section 4 and a summary is made in section 5.

2. Methodology

Each of the N pixels in an image χ is represented by its intensity x_i, $i=1,\ldots,N$. A threshold t partitions the image into two classes $C_1(t)$ and $C_2(t)$, where $C_1(t)=\{i\colon 0\le x_i\le t,\ 1\le i\le N\}$ and $C_2(t)=\{i\colon t<x_i\le T,$

☆ This paper has been recommended for acceptance by Aleix Martinez.

* Corresponding author. Tel.: +44 20 7679 1863; fax: +44 20 3108 3105.
E-mail addresses: jinghao@stats.ucl.ac.uk (J.-H. Xue), michael.titterington@gla.ac.uk (D.M. Titterington).

0262-8856/$ – see front matter © 2011 Elsevier B.V. All rights reserved.
doi:10.1016/j.imavis.2011.06.003

$1 \le i \le N\}$, in which T is the largest possible intensity, which is 255 for an 8-bit grey-level image (i.e. $x_i \in [0, T]$).

The histogram for the image χ, denoted by $\{h(x)\}$, can be constructed by counting the frequencies of the intensities and dividing them by N, such that $\sum_{x=0}^{T} h(x) = 1$.

2.1. Otsu's method and its median-based extension

2.1.1. Otsu's method

Otsu's rule [12,9] for defining the optimal threshold t can be written as

$$t_O^* = \underset{t}{\operatorname{argmin}} J_O(t) = \underset{t}{\operatorname{argmin}} \left\{ \omega_1(t) s_1^2(t) + \omega_2(t) s_2^2(t) \right\}, \quad (1)$$

where $\omega_1(t)$ and $\omega_2(t)$ are the proportions of pixels representing classes $C_1(t)$ and $C_2(t)$ determined by a threshold t, $s_1(t)$ and $s_2(t)$ are the (biased) sample standard deviations for $C_1(t)$ and $C_2(t)$, respectively, defined as

$$\omega_1(t) = \sum_{x=0}^{t} h(x),\ \omega_2(t) = \sum_{x=t+1}^{T} h(x) = 1 - \omega_1(t), \quad (2)$$

$$s_1^2(t) = \sum_{x=0}^{t} \left[\frac{h(x)}{\omega_1(t)} \{x - \bar{x}_1(t)\}^2 \right],\ s_2^2(t) = \sum_{x=t+1}^{T} \left[\frac{h(x)}{\omega_2(t)} \{x - \bar{x}_2(t)\}^2 \right], \quad (3)$$

in which $\bar{x}_1(t) = \sum_{x=0}^{t} \{x h(x) / \omega_1(t)\}$ and $\bar{x}_2(t) = \sum_{x=t+1}^{T} \{x h(x) / \omega_2(t)\}$ are the sample means for $C_1(t)$ and $C_2(t)$, respectively.

2.1.2. A median-based extension

As mentioned in section 1, we envisage that the use of the median instead of the mean may provide a t that is more robust to the presence of skew and heavy-tailed distributions for C_k than those selected by Otsu's method and the MET method. Therefore, a median-based extension of Otsu's method, derived in a natural way by substituting the MAD for s^2 (not for s for theoretical reasons explained in section 3), provides a rule for selecting t (denoted by g for distinctive purposes hereafter) as follows:

$$g_O^* = \underset{t}{\operatorname{argmin}} J_O^M(t) = \underset{t}{\operatorname{argmin}} \{\omega_1(t) MAD_1(t) + \omega_2(t) MAD_2(t)\}, \quad (4)$$

where $\mathrm{MAD}_k(t)$, the mean absolute deviation from the median for class $C_k(t)$, is given, for $k = 1, 2$, by

$$MAD_1(t) = \sum_{x=0}^{t} \left\{ \frac{h(x)}{\omega_1(t)} |x - m_1(t)| \right\}, \quad (5)$$

$$MAD_2(t) = \sum_{x=t+1}^{T} \left\{ \frac{h(x)}{\omega_2(t)} |x - m_2(t)| \right\}, \quad (6)$$

in which $m_1(t) = \mathrm{med}\{x_i : i \in C_1(t)\}$ and $m_2(t) = \mathrm{med}\{x_i : i \in C_2(t)\}$ are the sample medians for $C_1(t)$ and $C_2(t)$, respectively.

2.1.3. Multi-level thresholding

When there are more than two classes predetermined for an image (i.e. $K > 2$), it would be better to use more than one threshold to partition the image into these classes, leading to a multi-level thresholding problem.

For multi-level thresholding, Otsu's rule for selecting optimal thresholds $\mathbf{t}^* = (t_1^*, \ldots, t_{K-1}^*)$ can be written as

$$t_O^* = \underset{\mathbf{t}}{\operatorname{argmin}} \sum_{k=1}^{K} \left\{ \omega_k(\mathbf{t}) s_k^2(\mathbf{t}) \right\}, \quad (7)$$

where, similarly to the version in section 1, $\omega_k(\mathbf{t})$ and $s_k^2(\mathbf{t})$ are defined for $C_k(\mathbf{t})$.

Therefore, for multi-level thresholding, the rule underlying Otsu's median-based extension becomes

$$g_O^* = \underset{\mathbf{t}}{\operatorname{argmin}} \sum_{k=1}^{K} \{\omega_k(\mathbf{t}) MAD_k(\mathbf{t})\}. \quad (8)$$

2.2. The MET method and its median-based extension

2.2.1. The MET method

The MET method [8] selects t^* as

$$t_M^* = \underset{t}{\operatorname{argmin}} J_M(t) = \underset{t}{\operatorname{argmin}} \left\{ \omega_1(t) log \frac{s_1(t)}{\omega_1(t)} + \omega_2(t) log \frac{s_2(t)}{\omega_2(t)} \right\}, \quad (9)$$

where $\omega_1(t)$, $\omega_2(t)$, $s_1(t)$ and $s_2(t)$, defined in Eqs. (2) and (3), are positive here.

2.2.2. A median-based extension

By analogy with section 1, the rule underlying a median-based extension of the MET method can be derived by substituting the MAD for s (not as with section 2 for s^2 for theoretical reasons explained in section 3) as

$$g_M^* = \underset{t}{\operatorname{argmin}} J_M^M(t) = \underset{t}{\operatorname{argmin}} \left\{ \omega_1(t) log \frac{MAD_1(t)}{\omega_1(t)} + \omega_2(t) log \frac{MAD_2(t)}{\omega_2(t)} \right\}. \quad (10)$$

2.2.3. Multi-level thresholding

The multi-level-thresholding versions of the MET method and its median-based extension are readily given by

$$\mathbf{t}_M^* = \underset{\mathbf{t}}{\operatorname{argmin}} \sum_{k=1}^{K} \left\{ \omega_k(\mathbf{t}) log \frac{s_k(\mathbf{t})}{\omega_k(\mathbf{t})} \right\}, \quad (11)$$

$$g_M^* = \underset{\mathbf{t}}{\operatorname{argmin}} \sum_{k=1}^{K} \left\{ \omega_k(\mathbf{t}) log \frac{MAD_k(\mathbf{t})}{\omega_k(\mathbf{t})} \right\}. \quad (12)$$

3. Theoretical interpretation

3.1. Relationship with Laplace mixtures

A straightforward and intuitive interpretation of Otsu's rule, as shown in Eq. (1), is that it aims to minimise the within-classes variance $J_O(t)$, a measure of dispersion, of the intensity. Correspondingly, an interpretation of the median-based extension of Otsu's method, as shown in Eq. (4), is that the extension aims to minimise the within-classes mean absolute deviation from the median $J_O^M(t)$, another measure of dispersion, of the intensity.

Alternatively and insightfully, as mentioned in section 1, [9] shows that both Otsu's method and the MET method can be derived from maximisation of log-likelihoods based on mixtures of Gaussian distributions. The same type of interpretation can be found in [8] from the derivation of the MET method, although it was not explicitly mentioned there. Analogously to that, we present a similar theoretical interpretation of the median-based approaches, from the perspective of the maximisation of log-likelihoods based on mixtures of Laplace distributions.

Suppose that the intensity of class C_k follows a Laplace distribution, of which the probability density function $p(x|C_k)$ is defined as

$$p(x|C_k) = \frac{1}{2\beta_k} exp\left(- \frac{|x - \alpha_k|}{\beta_k} \right), \quad (13)$$

where α_k is a location parameter and β_k is a positive scale parameter. The maximum likelihood estimator (MLE) of α_k is the sample median

m_k for C_k, and the MLE of β_k is MAD_k, the mean absolute deviation from the median for C_k.

Without loss of generality, here we only consider the case of image binarisation (i.e. into C_1 and C_2).

In this case, the log-likelihood based on the joint distribution of the intensity and its class indicator can be written as

$$\ell(\theta(t)) = \sum_{x=0}^{t}\left[h(x)N\left\{log(p_1(t)) - log(2\beta_1(t)) - \frac{|x-\alpha_1(t)|}{\beta_1(t)}\right\}\right] + \sum_{x=t+1}^{T}\left[h(x)N\left\{log(p_2(t)) - log(2\beta_2(t)) - \frac{|x-\alpha_2(t)|}{\beta_2(t)}\right\}\right], \quad (14)$$

where $\theta(t)=\{\alpha_1(t),\ \beta_1(t),\ \alpha_2(t),\ \beta_2(t)\}$, and $p_k(t)$ is the prior probability of class $C_k(t)$, of which the MLE is the proportion $\omega_k(t)$.

As we have mentioned, the MLEs of $p_k(t)$, $\alpha_k(t)$ and $\beta_k(t)$ are $\omega_k(t)$, $m_k(t)$ and $\mathrm{MAD}_k(t)$, respectively, as shown in Eqs. (2), (5) and (6). Plugging them into Eq. (14), we obtain

$$\begin{aligned}\max_{\theta(t)}\frac{\ell(\theta(t))}{N} &= \omega_1(t)log(\omega_1(t)) - \omega_1(t)log(2MAD_1(t)) - \omega_1(t) \\ &\quad + \omega_2(t)log(\omega_2(t)) - \omega_2(t)log(2MAD_2(t)) - \omega_2(t), \quad (15)\\ &= \omega_1(t)log\frac{\omega_1(t)}{MAD_1(t)} + \omega_2(t)log\frac{\omega_2(t)}{MAD_2(t)} - 1 - log2.\end{aligned}$$

Therefore, we can select as the optimal g^* that which provides the largest maximum log-likelihood, as follows:

$$g^* = \operatorname*{argmax}_t\left\{\omega_1(t)log\frac{\omega_1(t)}{MAD_1(t)} + \omega_2(t)log\frac{\omega_2(t)}{MAD_2(t)}\right\}, \quad (16)$$

which equals g^*_M in Eq. (10), the threshold selected by the median-based extension of the MET method. This provides an interpretation for the extension.

When we consider the log-likelihood based only on the class-conditional distribution $p(x|C_k)$, in Eq. (14) the terms related to $log(p_k(t))$ disappear. We further assume that $\beta_1(t)=\beta_2(t)=\beta_w(t)$ such that $\beta_w(t)$ is estimated by the within-classes mean absolute deviation from the median, which is calculated as $\omega_1(t)MAD_1(t)+\omega_2(t)MAD_2(t)$. Consequently, based on a similar derivation to that leading from Eq. (14) to Eq. (16), we can readily obtain the median-based extension of Otsu's method, as stated in Eq. (4).

This also explains why we substitute the MAD for s^2 when we derive the extension of Otsu's method, while substituting the MAD for s when we derive the extension of the MET method.

In short, the two median-based approaches can be theoretically interpreted and justified, by modelling the histogram as a mixture of Laplace distributions.

3.2. Mixtures of non-Gaussian distributions

Researchers have developed various image-thresholding methods, which model the histogram as a mixture of non-Gaussian distributions, such as Poisson distributions [13], generalised Gaussian distributions [1,2], skew-normal and log-concave distributions [19] and certain distributions derived from Rayleigh [20], Nakagami-gamma, log-normal and Weibull distributions [11].

Some of these distributions, such as the generalised Gaussian distribution and the log-concave distribution, include the Laplace distribution as a special case. Fitting a mixture of such relatively generic distributions is complicated in both theoretical and computational terms; nevertheless, it may still be justified in certain practical contexts.

4. Discussion

4.1. Computational efficiency

The median-based approaches preserve not only the methodological simplicity and theoretical elegance, but also the computational efficiency, of their original methods.

It is a natural concern that the calculation of a median is often slower than that of a mean; the exhaustive search of the range of candidate thresholds for an optimal g^* makes this concern more prominent, because a considerable number of medians have to be calculated. Fortunately, by sorting all pixels once in descending or ascending order of their intensities before the search, the medians $m_k(t)$ for any candidate threshold t can easily be retrieved. Hence, the median-based approaches have little additional computational overheads, compared with their original mean-based methods.

4.2. Thresholding performance

4.2.1. Real images

To compare Otsu's method, the MET method and their median-based extensions, we choose four real test images, namely 'Lymp', 'NDT-image20', 'Lake' and 'Girlface'. The test images are publicly available: 'Lymp' comes with the software ImageJ (rsb.info.nih.gov/ij); 'Lake' and 'Girlface' are two benchmark test images; and 'NDT-image20' is a nondestructive-testing (NDT) image employed in a recent comprehensive survey of image-thresholding methods [16]. These images also feature in some image binarisation and multi-level thresholding literature including [14,5,6] and our recent pieces of work [18,19].

'Lymp' and 'NDT-image20' were chosen for binarisation; 'Lake' and 'Girlface' were used for tri-level thresholding. The results are displayed in Figs. 1 and 2, respectively.

Fig. 1 shows that, in both 'Lymp' and 'NDT-image20', the two classes are distinct in size, intensity range and skewness. In 'Lymp', the minority class (C_1, which is for the dark and approximately elliptical cells) has more skewed and widely-ranging intensities; in 'NDT-image20', the majority class (C_2, which is for the particles) has more skewed and dispersed intensities. The results of thresholds, superimposed as dashed lines on to the histograms, indicate the following features: for both images, the performance of the median-based extension of Otsu's method is slightly superior to that of the original Otsu method; and the performances of the MET method and its extension are rather similar.

In the histograms shown in Fig. 2 for 'Lake' and 'Girlface', there are three clearly-noticeable modes and one or more classes with skew distributions of intensity. From Fig. 2, we can also make the following observations. First, for 'Lake', only the median-based extension of the MET method successfully identified the three classes represented by the three modes of intensity. Secondly, in the case of 'Girlface', both extensions succeeded in distinguishing the three modes, as does the original Otsu method but not the original MET method.

In summary, for the binarisation and tri-level thresholding of the four test images, the median-based extensions perform more robustly than their original methods.

Nevertheless, bearing in mind the diversities of real images to be processed in practice and our intention to develop a relatively-robust thresholding approach, we shall use simulated data to investigate further the robustness of the median-based approaches.

4.2.2. Simulated data

Here we simulate three datasets, denoted by χ_1, χ_2 and χ_3, from mixtures of skew-Laplace distributions, using an R package *HyperbolicDist* (www.r-project.org). A skew-Laplace distribution is both skew

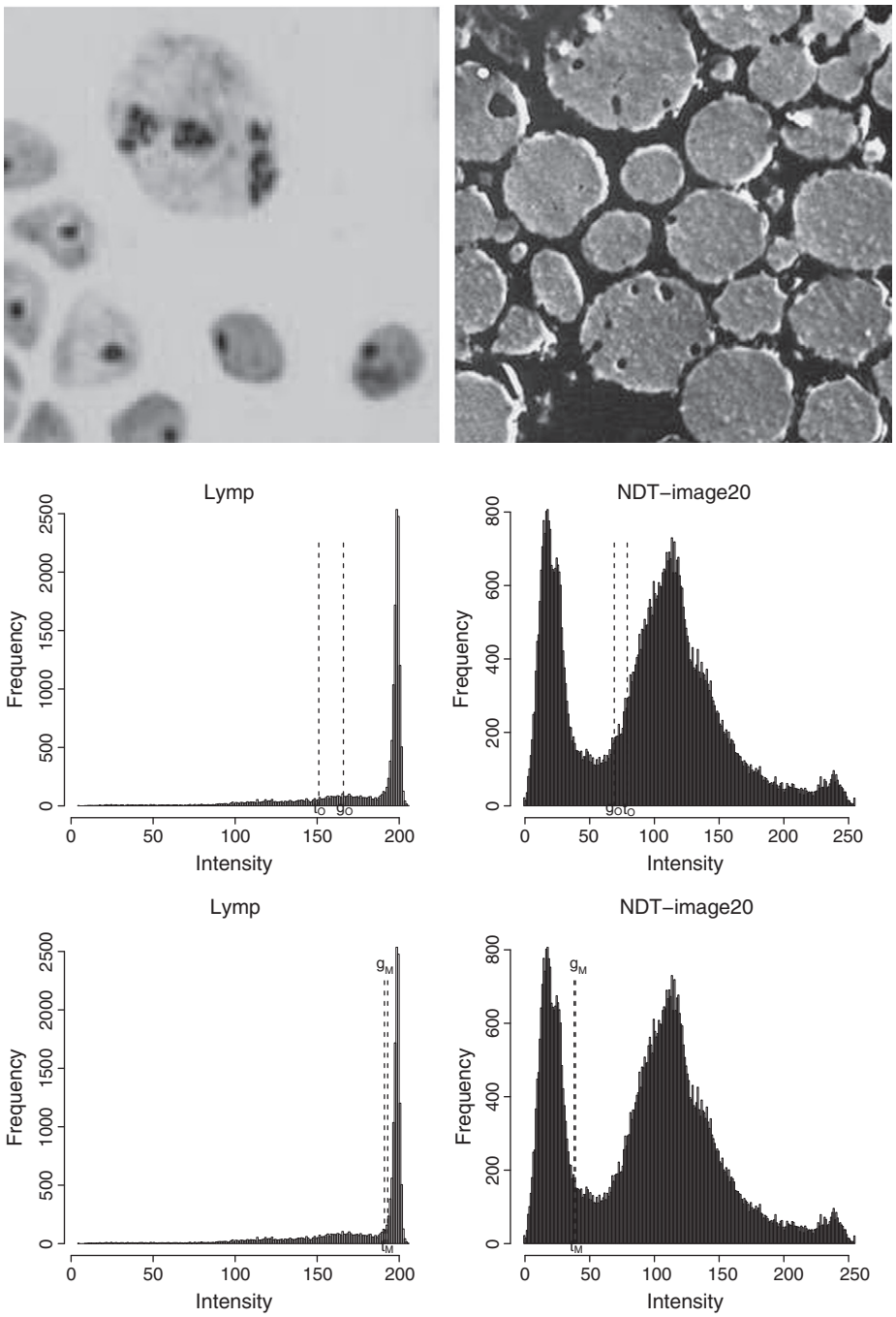

Fig. 1. Binarisation of real images. Left-hand column: for 'Lymp'; right-hand column: for 'NDT-image20'. Upper row: original images. Middle row: histograms with thresholds t^*_O (selected by Otsu's method) and g^*_O (by the median-based Otsu method). Lower row: histograms with thresholds t^*_M (selected by the MET method) and g^*_M (by the median-based MET method). Thresholds are indicated by dashed lines.

and heavy-tailed [3]; by using the notation in Eq. (13), its probability density function can be written as

$$p(x|C_k) = \begin{cases} (\beta_{kl} + \beta_{kr})^{-1} exp\{(x-\alpha_k)/\beta_{kl}\} & \text{if } x \le \alpha_k, \\ (\beta_{kl} + \beta_{kr})^{-1} exp\{-(x-\alpha_k)/\beta_{kr}\} & \text{if } x > \alpha_k, \end{cases} \quad (17)$$

where α_k is a location parameter for the mode, and β_{kl} and β_{kr} are two positive scale parameters for the left and right parts of the density function for class C_k, respectively. It reverts to the symmetric Laplace distribution in Eq. (13) when $\beta_{kl} = \beta_{kr}$, but is skew otherwise.

For dataset χ_1, the settings are $\omega_1 = 0.5$, $\alpha_1 = 150$, $\alpha_2 = 175$, $\beta_{1l} = 20$, $\beta_{1r} = 2$, $\beta_{2l} = \beta_{2r} = 10$, such that classes C_1 and C_2 are equal-sized and overlapping, with C_1 skew but C_2 symmetric. Starting from χ_1, we adopt $\frac{\beta_{2r}}{2}$ and $\frac{\beta_{2r}}{4}$ to construct χ_2 and χ_3, respectively; that is, C_2 becomes more skew from χ_1 to χ_3, as shown in Fig. 3.

From the left-hand column of Fig. 3, we observe that Otsu's method performs worse from χ_1 to χ_3 while its median-based extension behaves more robustly. From the right-hand column of Fig. 3, we observe that the MET method performs worse from χ_3 to χ_1 while its median-based extension acts more robustly. In short, for these three

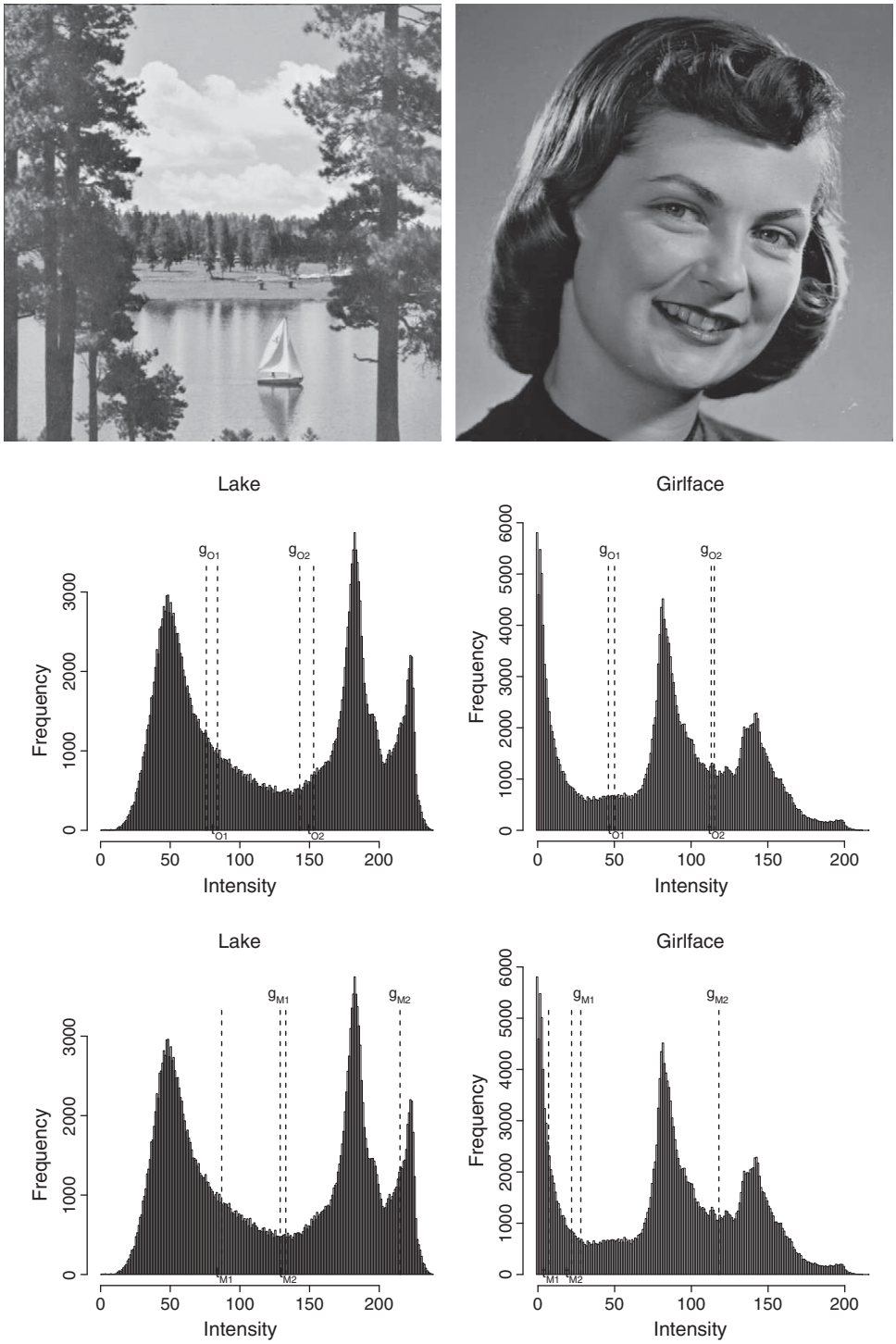

Fig. 2. Tri-level thresholding of real images. Left-hand column: for 'Lake'; right-hand column: for 'Girlface'. The rest of the caption is as in Fig. 1.

datasets containing skew, heavy-tailed and overlapping data, the performance of the median-based approaches is relatively robust.

We note that these data are presented mainly for illustrative purposes; for such data, some other methods including those based on valley seeking may also achieve robust performance.

4.3. Some limitations

Here we discuss two limitations of the approaches studied in this paper: one is the multi-modality of the criterion functions $J_O(t)$, $J_O^M(t)$, $J_M(t)$ and $J_M^M(t)$; the other is the extreme results of t^*_M and g^*_M.

The first limitation can be illustrated by plotting $J_M(t)$ in Eq. (9) for χ_2 (or χ_1), for which the MET method does not perform well. As displayed in the left-hand column of Fig. 4, $J_M(t)$ is multi-modal and the local minimum at about 160 indicates a better threshold than does the global minimum at about 90. Such a problem resulting from multi-modality is also associated with the functions $J_O(t)$, $J_O^M(t)$ and $J_M^M(t)$.

Indeed, it was demonstrated in [7,10] that the between-class variance, or equivalently the within-class variance $J_O(t)$, is not necessarily unimodal for Otsu's method, and, more importantly, in such a multi-modal case the global extremum is not guaranteed to be

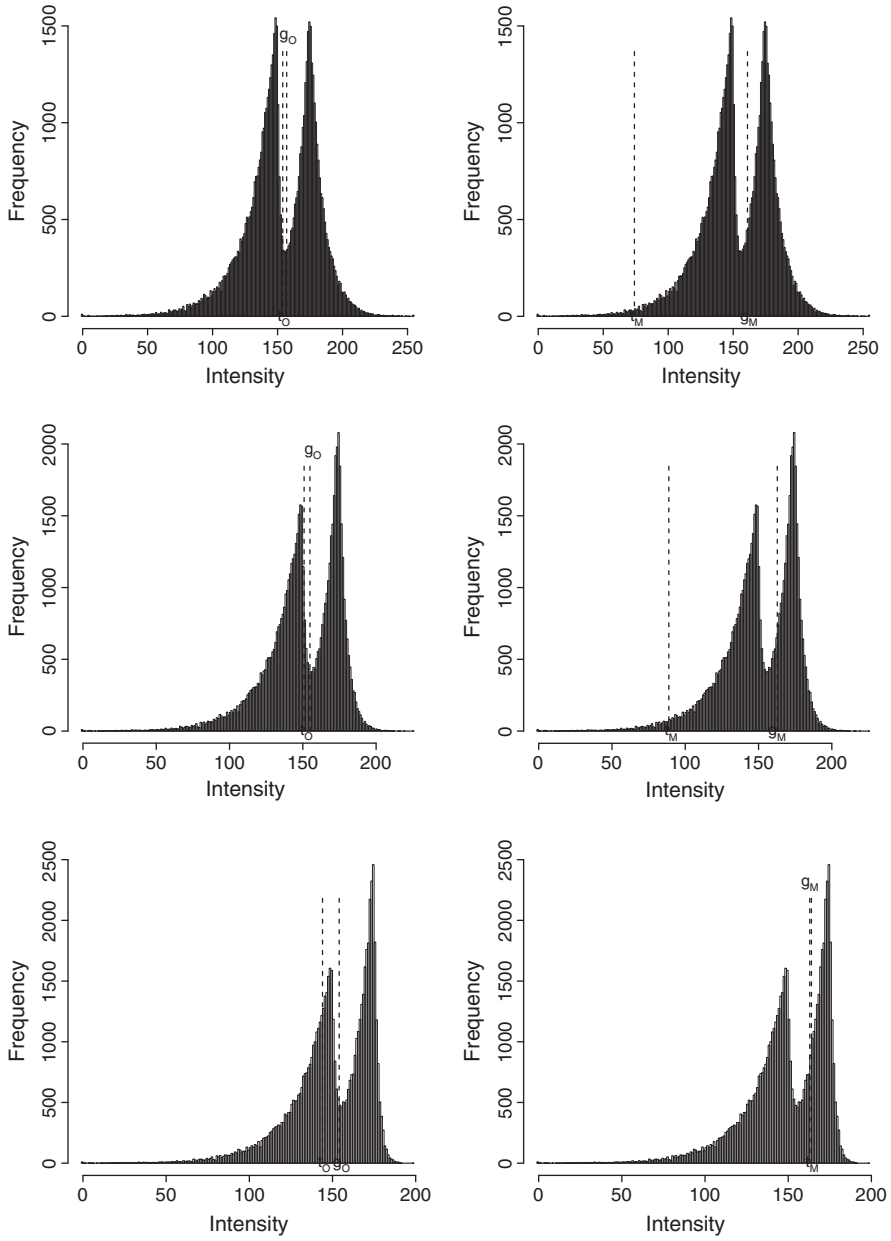

Fig. 3. Binarisation of simulated data. Left-hand column: thresholds t^*_O and g^*_O obtained by Otsu's method and its median-based extension; right-hand column: thresholds t^*_M and g^*_M obtained by the MET method and its median-based extension. Upper row: for χ_1; middle row: for χ_2; lower row: for χ_3.

a better threshold than a local extremum. For illustrative purposes, [7,8] simulate data from a two-component Gaussian mixture, where the two components (or classes) have greatly disparate sizes (with a ratio of 99 to 1). To enhance their observations, we follow their setting of parameters for the mixture but use a two-component Laplace mixture. The results are shown in the right-hand column of Fig. 4, from which we can observe that, for Otsu's method and its median-based extension, the local minima of $J_O(t)$ and $J^M_O(t)$ at around 125 provide a better threshold than does the global minima at about 90.

To solve this problem, we may carry out a simple "valley check" suggested in [7] to ignore a threshold t^* that does not satisfy $h(t^*)<h(\bar{x}_1(t^*))$ and $h(t^*)<h(\bar{x}_2(t^*))$.

The second limitation can be illustrated by Eqs. (9) and (10), where the term $logs_k(t)$ or $log\ MAD_k(t)$ tends to favour a homogeneous class with tiny dispersion (i.e. with few intensities), resulting in thresholds t^*_M and g^*_M that are extreme, towards the ends of the intensity range.

To overcome this limitation, it may be worthwhile to check the size of each class after thresholding by the MET method and its median-based extension. If a resulting class is too small, Otsu's method or its median-based extension can be employed as an alternative or as an initial step to constrain the search range for the MET methods. The idea of using Otsu's method to initiate the MET method was recommended for their iterative versions by [22].

5. Summary

We have proposed two median-based approaches to image thresholding, to extend Otsu's method and Kittler and Illingworth's MET method. We have provided theoretical interpretation of the new

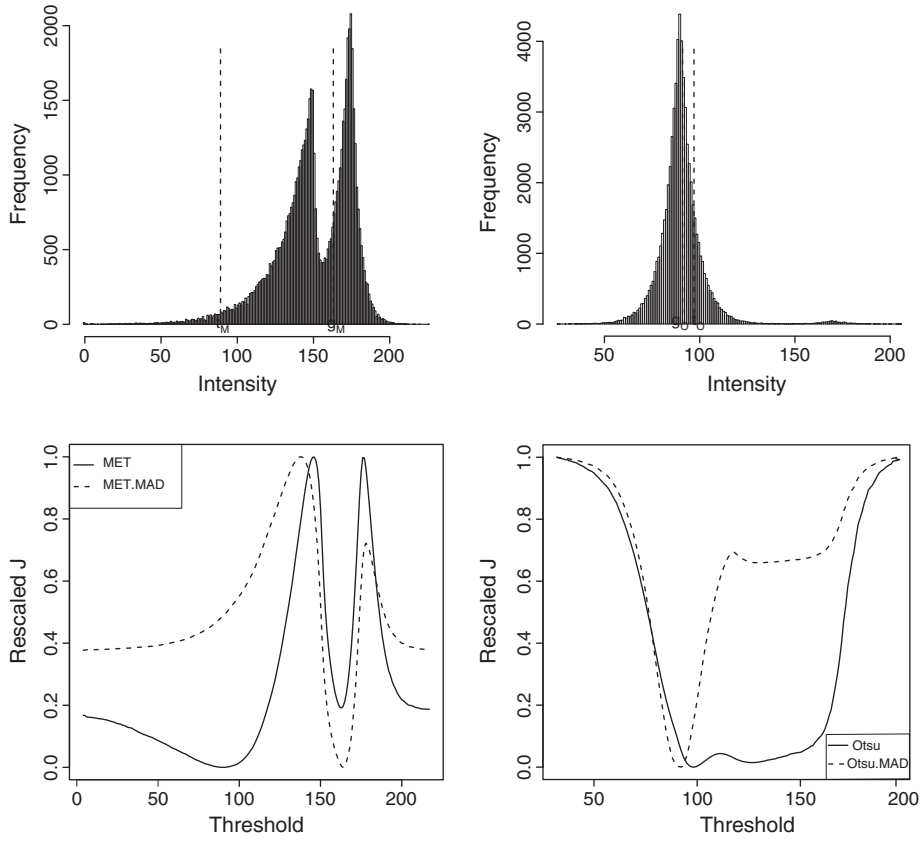

Fig. 4. Thresholds and $J(t)$ for Otsu's method, the MET method and their median-based extensions for mixtures of two Laplace distributions. Right-hand column: for Otsu's method and its extension; left-hand column: for the MET method and its extension. Upper row: histograms with thresholds. Lower row: $J(t)$ rescaled to the range [0, 1].

approaches, based on mixtures of Laplace distributions. We have shown that the two extensions preserve the methodological simplicity and computational efficiency of their original methods, and can in general achieve more robust performance for skew and heavy-tailed data.

Acknowledgments

The NDT images are provided through the courtesy of Dr. Mehmet Sezgin. This work was partly supported by funding to J.-H.X. from the Internal Visiting Programme of the EU-funded PASCAL2 Network of Excellence. We are grateful for the referees' generous and constructive suggestions.

References

[1] Y. Bazi, L. Bruzzone, F. Melgani, Image thresholding based on the EM algorithm and the generalized Gaussian distribution, Pattern Recognition 40 (2) (2007) 619–634.
[2] S.-K.S. Fan, Y. Lin, C.-C. Wu, Image thresholding using a novel estimation method in generalized Gaussian distribution mixture modeling, Neurocomputing 72 (1–3) (2008) 500–512.
[3] N.R.J. Fieller, E.C. Flenley, W. Olbricht, Statistics of particle size data, Journal of the Royal Statistical Society. Series C (Applied Statistics) 41 (1) (1992) 127–146.
[4] C.A. Glasbey, An analysis of histogram-based thresholding algorithms, CVGIP: Graphical Models and Image Processing 55 (6) (1993) 532–537.
[5] R. Guo, S.M. Pandit, Automatic threshold selection based on histogram modes and a discriminant criterion, Machine Vision and Applications 10 (5–6) (1998) 331–338.
[6] K. Hammouche, M. Diaf, P. Siarry, A comparative study of various meta-heuristic techniques applied to the multilevel thresholding problem, Engineering Applications of Artificial Intelligence 23 (5) (2010) 676–688.
[7] J. Kittler, J. Illingworth, On threshold selection using clustering criteria, IEEE Transactions on Systems, Man, and Cybernetics SMC 15 (5) (1985) 652–655.
[8] J. Kittler, J. Illingworth, Minimum error thresholding, Pattern Recognition 19 (1) (1986) 41–47.
[9] T. Kurita, N. Otsu, N. Abdelmalek, Maximum likelihood thresholding based on population mixture models, Pattern Recognition 25 (10) (1992) 1231–1240.
[10] H. Lee, R.-H. Park, Comments on "An optimal multiple threshold scheme for image segmentation", IEEE Transactions on Systems, Man, and Cybernetics 20 (3) (1990) 741–742.
[11] G. Moser, S.B. Serpico, Generalized minimum-error thresholding for unsupervised change detection from SAR amplitude imagery, IEEE Transactions on Geoscience and Remote Sensing 44 (10) (2006) 2972–2982.
[12] N. Otsu, A threshold selection method from gray-level histograms, IEEE Transactions on Systems, Man, and Cybernetics SMC 9 (1979) 62–66.
[13] N.R. Pal, D. Bhandari, Image thresholding: some new techniques, Signal Processing 33 (2) (1993) 139–158.
[14] P.K. Sahoo, G. Arora, Image thresholding using two-dimensional Tsallis–Havrda–Charvát entropy, Pattern Recognition Letters 27 (6) (2006) 520–528.
[15] P.K. Sahoo, S. Soltani, A.K.C. Wong, Y.C. Chen, A survey of thresholding techniques, Computer Vision, Graphics, and Image Processing 41 (2) (1988) 233–260.
[16] M. Sezgin, B. Sankur, Survey over image thresholding techniques and quantitative performance evaluation, Journal of Electronic Imaging 13 (1) (2004) 146–165.
[17] Ø.D. Trier, A.K. Jain, Goal-directed evaluation of binarization methods, IEEE Transactions on Pattern Analysis and Machine Intelligence 17 (12) (1995) 1191–1201.
[18] J.-H. Xue, D.M. Titterington, Image thresholding by using some statistics for determining the number of clusters, , 2011 manuscript.
[19] J.-H. Xue, D.M. Titterington, Threshold selection from image histograms with skewed components based on maximum-likelihood estimation of skew-normal and log-concave distributions, , 2011 manuscript.
[20] J.-H. Xue, Y.J. Zhang, X.G. Lin, Rayleigh-distribution based minimum error thresholding for SAR images, Journal of Electronics (China) 16 (4) (1999) 336–342.
[21] H. Yan, Unified formulation of a class of image thresholding techniques, Pattern Recognition 29 (12) (1996) 2025–2032.
[22] Q.-Z. Ye, P.-E. Danielsson, On minimum error thresholding and its implementations, Pattern Recognition Letters 7 (4) (1988) 201–206.